# Spin-Nematic Interaction in the Multiferroic Compound $Ba_2CoGe_2O_7$

M. Soda,[1] M. Matsumoto,[2] M. Månsson,[3,4] S. Ohira-Kawamura,[5] K. Nakajima,[5] R. Shiina,[6] and T. Masuda[1,*]
[1]Neutron Science Laboratory, Institute for Solid State Physics, University of Tokyo, Tokai, Ibaraki 319-1106, Japan
[2]Department of Physics, Shizuoka University, Shizuoka 422-8529, Japan
[3]Laboratory for Quantum Magnetism (LQM), École Polytechnique Fédérale de Lausanne (EPFL), Station 3, CH-1015 Lausanne, Switzerland
[4]Laboratory for Neutron Scattering, Paul Scherrer Institut, CH-5232 Villigen PSI, Switzerland
[5]Materials and Life Science Division, J-PARC Center, Tokai, Ibaraki 319-1195, Japan
[6]Department of Materials Science and Technology, Niigata University, Niigata 950-2181, Japan
(Received 22 January 2014; published 26 March 2014)

We demonstrate the existence of the spin-nematic interactions in an easy-plane type antiferromagnet $Ba_2CoGe_2O_7$ by exploring the magnetic anisotropy and spin dynamics. The combination of neutron scattering and magnetic susceptibility measurements reveals that the origin of the in-plane anisotropy is an antiferro-type interaction of the spin-nematic operator. The relation between the nematic operator and the electric polarization in the ligand symmetry of this compound is presented. The introduction of the spin-nematic interaction is useful to understand the physics of spin and electric dipole in multiferroic compounds.

DOI: 10.1103/PhysRevLett.112.127205 PACS numbers: 75.85.+t, 61.05.F-, 75.25.-j, 75.40.Gb

Symmetry breaking of time reversal and space inversion allows spontaneous order both in magnetism and dielectricity [1]. The enhanced simultaneous order, multiferroics [2,3], has been extensively studied since the discovery of its experimental realization in the perovskite manganite $TbMnO_3$ [4]. The microscopic consideration of electronic states taking into account a spin-orbit interaction and symmetry of crystals reveals the relationship between the structures of spin $\boldsymbol{S}$ and polarization $\boldsymbol{P}$ [5–9]. So far, in many multiferroic materials, the stability of complex spin orders has been focused in relation with induced electric polarizations. On the other hand, existence of an interaction among electric polarizations and its interplay with the spin interaction still remains unclear. In this context, a new material $Ba_2CoGe_2O_7$ provides a simple and quite interesting playground in which the polarizations are described by a rank two symmetric tensor of local spin operators, reflecting a symmetry of the tetrahedral unit involving the magnetic Co ions. One may call the spin representation of the polarization nematic or quadrupole, and can analyze their interaction on an equal footing with the spin exchange interaction. The main purpose of this Letter is to give convincing evidence of realizing the nematic interaction and to clarify its crucial role in the magnetic anisotropy and the low energy physics in $Ba_2CoGe_2O_7$.

The two-dimensional square lattice antiferromagnet $Ba_2CoGe_2O_7$ includes a metal-ligand motif with high symmetry but without an inversion center. The crystal structure is tetragonal $P\bar{4}2_1m$ as schematically shown in Fig. 1(a). $Co^{2+}$ ions carry spin $S = 3/2$ and the $CoO_4$ tetrahedron is distorted along the $c$ direction. The compound exhibits an antiferromagnetic transition at $T_N = 6.7$ K [10] and a staggered antiferromagnetic structure in the (001) plane with slight canting [11]. Below $T_N$, an electric polarization induced by a magnetic field is observed [12–14]. The origin of the polarization was explained by a spin-dependent $d$-$p$ hybridization mechanism [12].

The electrons in the Co ion at the center of an isolated $O_4$ tetrahedron suffer from a crystal field potential of the point group $D_{2d}$. In this case, as we shall show later, conventional spin interaction does not break the spin rotation symmetry in the plane (001). In the present study, however, the combination of inelastic neutron scattering with high energy resolution and magnetic susceptibility measurements in $Ba_2CoGe_2O_7$ reveals existence of the distinct anisotropy in the plane. We argue through the following study that an unconventional nematic interaction is the origin of the anisotropy.

Stoichiometric quantities of $BaCO_3$, CoO, and $GeO_2$ powders were mixed and sintered at 900° C for 24 h. The obtained powder is pressed into rods and they were sintered at 1000° C for 24 h. Using these rods as starting materials, single crystals were grown in air at a rate of 1 mm/$h$ by the floating zone method. Typical dimension of the crystals is about 8 mm in diameter and 40 mm in length. We confirmed the absence of the impurity phase by using a powder x-ray diffractometer. Bulk magnetization was measured using a conventional SQUID magnetometer. Neutron measurements were carried out using the cold-neutron triple axis spectrometer TASP installed at SINQ/PSI, Switzerland. Throughout this Letter, we use the tetragonal unit cell with $a = b = 8.410$ and $c = 5.537$ Å. The scattering plane was the $a$-$c$ plane. The final neutron energy was set at 5 meV. The magnetic fields were applied along

 

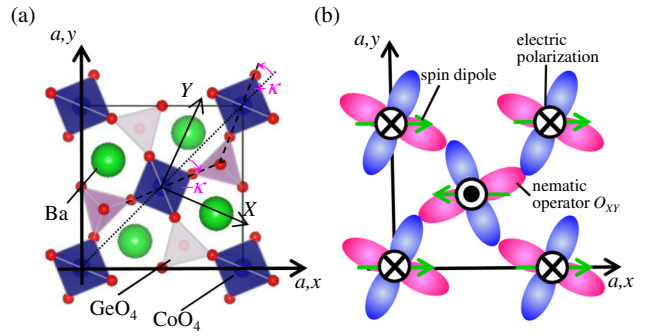


FIG. 1 (color online). (a) Crystal structure of $Ba_2CoGe_2O_7$ . $CoO_4$ tetrahedra separated by $GeO_4$ tetrahedra form a square lattice in the (001) plane. The $x$ and $y$ axes in the global coordinate of spin are defined along the [100] and [010] directions. The $X$ and $Y$ axes are locally defined on each$CoO_4$ tetrahedron. (b) Structures of spin dipoles, spin-nematic operator $O_{XY}$, and electric polarizations at zero magnetic field in $Ba_2CoGe_2O_7$ .

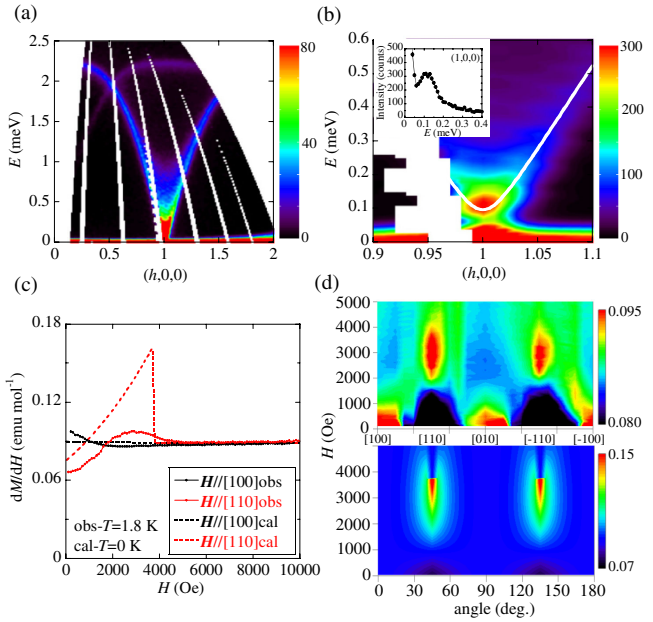


FIG. 2 (color online). (a) Inelastic neutron scattering spectrum obtained by using the AMATERAS spectrometer in J-PARC. Well-defined spin-wave excitations are observed. (b) Inelastic neutron scattering spectrum in the low energy range. The calculated dispersion is shown by the white solid curve. The inset shows the constant-$Q$ scan at $\mathbf{Q} = (1, 0, 0)$. (c) Bulk susceptibility $dM/dH$ measured at $T = 1.8$ K. Red and black symbols indicate the $dM/dH$ for $H\|$ [110] and $H\|$ [100], respectively. Field cooled processes are shown. Red and black dashed curves indicate the $dM/dH$ at $T = 0$ K calculated by mean-field theory. (d) The measured angular dependence of $dM/dH$ in the upper panel and the calculated ones in the lower panel.

a direction vertical to the scattering plane (magnetic field $H\|$) using a superconducting magnet. Neutron measurements were also carried out using a cold-neutron disk-chopper spectrometer AMATERAS of a direct geometry type installed at J-PARC, Japan. The chopper condition was set so that the incident neutron energies $E_i$ was 3.14 meV and the resolutions of the energy transfer at the elastic position was 0.075 meV.

In Fig. 2(a) the neutron spectrum is shown and a couple of spin-wave modes with the band energy of 2.2 meV are observed. Focused on the low energy range, a clear anisotropy gap of approximately 0.10 meV at the antiferromagnetic zone center $\boldsymbol{Q} = (1, 0, 0)$ is observed in Fig. 2(b). The magnetic susceptibilities $dM/dH$ in field applying along the [100] and [110] directions are shown in Fig. 2(c). In the latter, a peak due to a spin-flip (SF) transition is observed at $H \sim 3$ kOe that is consistent with the energy scale of the anisotropy gap, while in the former the SF transition is absent. The angular dependence of $dM/dH$ is summarized in the upper panel of Fig. 2(d), where fourfold rotational symmetry with the enhanced SF field at [110] and $[\bar{1}10]$ is observed. The presence of the fourfold in-plane anisotropy is consistent with the prediction of the anisotropy by investigating the crystallographic symmetry [15,16].

In general, the origin of the magnetic anisotropy gap in the excitation spectrum is a single-ion anisotropy or a two-ion anisotropy. The single-ion anisotropy in the spin state in this material is represented by the form $D(S^z)^2$ where the $z$ axis is the crystallographic $c$ axis. We note that there is no $E$ term in the tetragonal system. The sign of $D$ is believed to be positive since the direction of spins in the ordered state is perpendicular to the $c$ axis. Spin operators with 4th or higher order is inactive for $S = 3/2$ in the local symmtery and, thus, the single ion anisotropy cannot lead to any in-plane anisotropy. Consider next the nonlocal symmetry of Co ions located on the $2a$ Wyckoff positions in the space group $P\bar{4}2_1m$ and the allowed two-ion anisotropy represented by a spin-dipole interaction is an $XXZ$-type one $J^x(S_1^xS_2^x + S_1^yS_2^y) + J^zS_1^zS_2^z$. The anisotropy, again, does not break the rotational symmetry in the $c$ plane nor induce the anisotropy gap. Among the two-ion anisotropies that break the rotational symmetry, the one having the lowest order is represented by the interaction between spin-nematic (quadrupole) operators, of which the exact formula will be obtained later. This means that in $Ba_2CoGe_2O_7$ the spin-nematic interaction is the leading term for rotational symmetry broken and, hence, the origin of the observed anisotropy gap is the spin-nematic interaction.

The representation of spin-nematic interaction is obtained by considering the electric polarization interaction. In $Ba_2CoGe_2O_7$ the spin-nematic operator becomes equivalent to the polarization owing to the lack of the inversion symmetry in the $D_{2d}$ point-group symmetry of the$CoO_4$ tetrahedron [17,18]. Thus, $P^X = -K_{ab}O_{YZ}$, $P^Y = -K_{ab}O_{ZX}$, and $P^Z = -K_cO_{XY}$, where $K_{ab}$ and $K_c$ are constants and $X$, $Y$, and $Z$ are the local coordinates

onCoO$_4$ tetrahedron as shown in Fig. 1(a) [19]. Here the spin-nematic operator is defined as $O_{\alpha\beta} = S^\alpha S^\beta + S^\alpha S^\beta$, where $\{\alpha, \beta\} = \{X, Y, Z\}$. Let us consider the electrostatic polarization interaction on the basis of these operators. Among these, $O_{YZ}$ and $O_{ZX}$ become zero under the spin structure aligned in the $ab$ plane, while $O_{XY}$ is finite. Then, only the $Z$ component, $P^Z \propto O_{XY}$, is active and an intersite interaction of $P^Z$ is converted to a nematic interaction of $O_{XY}$ with an effective coupling strength $J_p^{\rm eff}$ [17]. The explicit form is

$$\mathcal{H}_p = -J_p \sum_{i,j} P^Z(i) P^Z(j) = -J_p^{\rm eff} \sum_{i,j} O_{XY}(i) O_{XY}(j). \tag{1}$$

Thus, intersite polarization interaction gives rise to the interaction between the spin-nematic operators. After the transformation to the global $xy$ coordinates, we obtain

$$O_{XY} = (\cos(2\kappa) O_{xy} - \sin(2\kappa) O_2^2), \tag{2}$$

where $O_{xy} = S^x S^y + S^y S^x$ and $O_2^2 = (S^x)^2 - (S^y)^2$ [17,20]. The definition of the angle $\kappa$ is described in Fig. 1(a). Calculation of the classical energy including antiferromagnetic spin interaction and the nematic interaction between $O_{XY}$ operators result in a ground state with staggered spin structure with fourfold rotational symmetry. Thus, the existence of the nematic interaction explains the biaxial magnetic anisotropy in our experiment.

The sign of $J_p$ and the magnetic-easy axes are determined from the angular dependence of the SF field $H_{\rm SF}$. In zero field there are four magnetic domain states; two of them share the magnetic easy axis and so do the rest two. The direction of the axis is orthogonal to each other. If the field is applied along one of the easy axes the spins in a domain of which the easy axis is parallel to the field flip instantly and those in another domain stay as they are. Hence, the value of $H_{\rm SF}$ is zero or strongly suppressed. As the field direction tilts from the easy axes the Zeeman energy required for the SF increases and, consequently, $H_{\rm SF}$ is enhanced. Experimentally, the minimum of $H_{\rm SF}$ is observed at $H\|$ [010] and [100] and this means that the easy axes are [010] and [100]. This magnetic anisotropy leads the negative sign of $J_p$ in Eq. (1), i.e., the antiferro-type nematic interaction that is equivalent to the antiferroelectric polarization. It is consistent with the zero polarization along the $Z$ direction at $H = 0$ Oe previously reported [12,13]. Indeed the calculation of the polarization curve assuming antiferroelectric polarization was consistent with the experiment [17]. The structure of the spin dipole, spin-nematic operator, and the electric polarization is depicted in Fig. 1(b).

To estimate the spin-nematic interaction $J_p^{\rm eff}$, we performed the calculation of magnetic dispersion relation and magnetic susceptibility as displayed in Figs. 2(b), 2(c), and 2(d). The main magnetic parameters including the exchange constant and single ion anisotropy along the $z$ direction are separately obtained; that will be explained later. The dispersion is reproduced by the main parameters plus $J_p^{\rm eff} = -0.198$ $\mu$eV as shown by the white solid curve. The calculated susceptibility by using the same parameters in the neutron spectrum is shown in the lower panel of Fig. 2(d) and it reasonably reproduces the experiment. Hence, the magnetic anisotropy observed both in the neutron spectrum and bulk magnetic susceptibility is consistently explained by introducing the antiferronematic spin interaction.

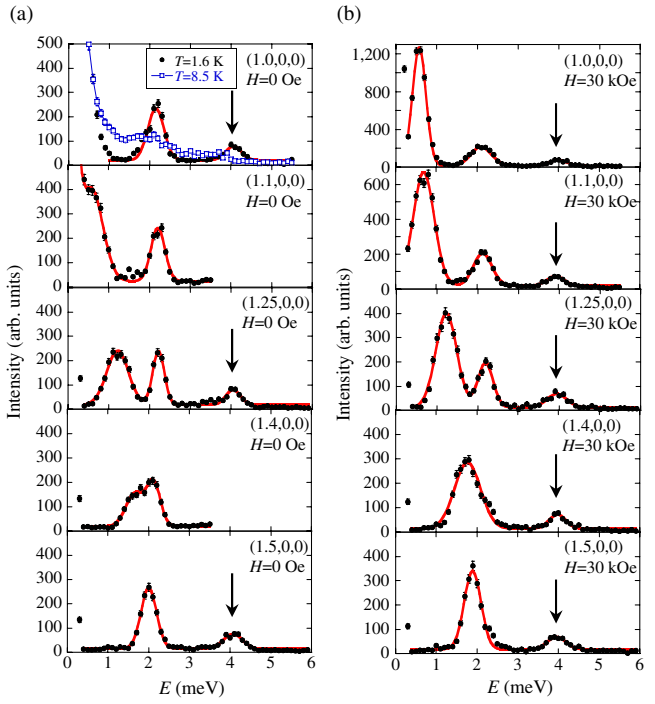


FIG. 3 (color online). Typical constant-$Q$ scans at $H = 0$ Oe and 30 kOe obtained by using the TASP spectrometer in PSI. Solid circles are the data at $T = 1.6$ K and open squares are those at $T = 8.5$ K. Red solid curves are fits to the data by Gaussian functions.

To determine the main magnetic parameters, inelastic neutron scattering spectra for extended energy transfers were measured as shown in Fig. 3. In addition to the low energy excitations at $0 \lesssim \hbar\omega \lesssim 2$ meV reported in a previous neutron scattering study [11], a new excitation at $\hbar\omega \sim 4$ meV is observed, which corresponds to an electric-field active mode confirmed by electromagnetic wave absorption experiments [20,21]. The excitation energies obtained by the Gaussian fits to the constant-Q scans are plotted in Figs. 4(a) and 4(c). Obtained intensities for the excitations are also plotted in Figs. 4(b) and 4(d). While the lower energy modes at $\hbar\omega \lesssim 2$ meV are explained by a classical spin-wave theory for a square-lattice antiferromagnet, the higher energy modes cannot be reproduced. To analyze all the modes we use extended spin-wave theory

[22] that is equivalent to the bond operator formulation [18,23,24]. We consider the Hamiltonian

$$\mathcal{H} = \sum_i \mathcal{H}_{\text{intra}}(i) + \sum_{\langle i,j \rangle} \mathcal{H}_{\text{inter}}(i,j), \tag{3}$$

where $\mathcal{H}_{\text{intra}}(i)$ and $\mathcal{H}_{\text{inter}}(i,j)$ are Hamiltonians for intrasite and intersite parts defined by

$$\mathcal{H}_{\text{intra}}(i) = D(S_i^z)^2 - \sum_{\alpha=x,y,z} g^\alpha \mu_B H^\alpha S_i^\alpha, \tag{4}$$

$$\mathcal{H}_{\text{inter}}(i,j) = \sum_{\alpha=x,y,z} J^\alpha S_i^\alpha S_j^\alpha + D_{\text{DM}}^z(i,j)(S_i^x S_j^y - S_i^y S_j^x) + \mathcal{H}_p. \tag{5}$$

Here, $S_i^\alpha$ is an $\alpha(=x,y,z)$ component of the $S=3/2$ spin operator at the $i$th site. In the presence of large $D$, the local energy eigenstates are split into two doublets of $S^z = \pm 1/2$ and $\pm 3/2$. For $D > 0$, $S^z = \pm 1/2$ doublet is stabilized and through intersite interaction an effective $S = 1/2$ spin wave is induced in the low energy range. Further, crystal-field-like excitation from $S^z = \pm 1/2$ to $\pm 3/2$ exists at higher energy.

As the result of neutron cross section analysis, we obtain the parameters summarized in Table I, which are semiquantitatively consistent with those obtained from ESR studies [18]. The spin system is approximately identified as $S = 3/2$ square-lattice antiferromagnet with large positive $D$. Calculated dispersion of the magnetic excitation along $\boldsymbol{Q} = (h,0,0)$ for $H = 0$ Oe and 30 kOe are shown in Figs. 4(a) and 4(c) by solid curves. The lowest and second lowest-lying modes are basically connected to the interacting lowest-lying doublets of the $S^z = \pm 1/2$. The former is the transverse fluctuation in the $a$-$b$ plane, $T_1$ mode and the latter are those in the $c$ direction, $T_2$ mode as depicted in Fig. 4(e). On the other hand, the mode around 4 meV comes from the higher-lying doublets and contains a large magnitude of longitudinal fluctuations of the ordered moment, $L$ mode [18,24], and a small magnitude of transverse fluctuations, $T_1$ and $T_2$ modes. These $L$, $T_1$, and $T_2$ modes are consistent with those identified in the previous ESR studies [18].

The existence of spin-nematic interaction in the multiferroic compound $Ba_2CoGe_2O_7$ was revealed for the first time by a combination of inelastic neutron scattering and bulk magnetization measurements. Several key features in this compound make the physics very interesting; strong spin-orbit interaction, the metal-ligand symmetry with no inversion center, and the absence of conventional in-plane anisotropy. In the course of this study, we have emphasized that such circumstances result in a characteristic correlation among spin nematic, spin dipole, electric polarization, which is totally described in the spin basis. Using this framework, we succeeded in determining the dielectric energy by measuring precisely the magnetic anisotropy energy.

From a magnetic point of view the electric field tunes the direction of the magnetic moment and the determined dielectric energy can be a performance index for multiferroicity. A further search for magnets that exhibit small magnetic anisotropy, and therefore small electric field for achieving ferroelectricity, would lead a practical

TABLE I. Parameters obtained by extended spin wave calculations.

| $J^x$, $J^y$ (meV) | $J^z$ (meV) | $D$ (meV) | $J_p^{\text{eff}}$ ($\mu$eV) | $D_{\text{DM}}^z$ ($\mu$eV) |
|---|---|---|---|---|
| 0.208 | 0.253 | 1.034 | −0.198 | 8.61 |

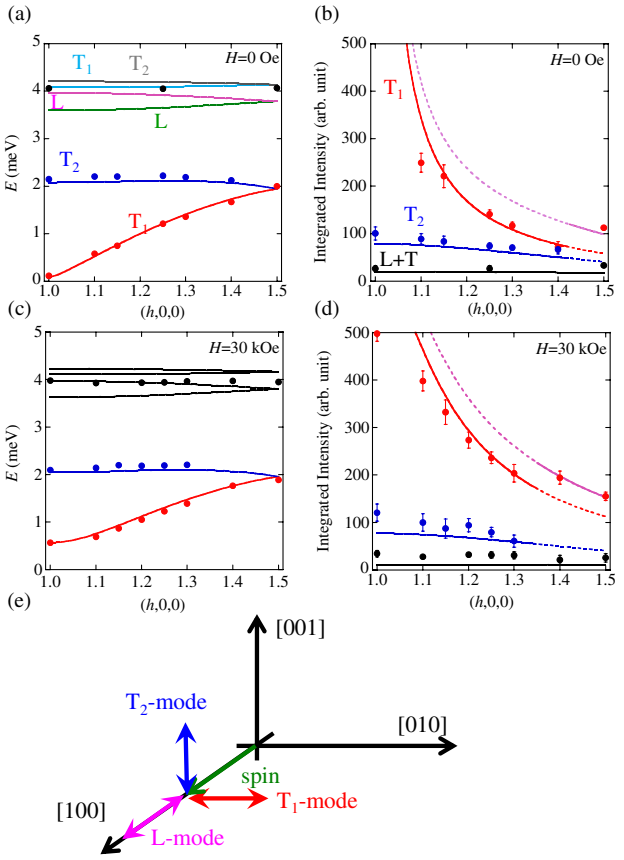


FIG. 4 (color online). (a) Magnon dispersion relation for $\mathbf{Q} = (h,0,0)$ at $H = 0$ Oe. (b) Intensity of the inelastic neutron scattering at $H = 0$ Oe. (c),(d) Magnon dispersion and intensity for $H = 30$ kOe. In each figure the theoretical calculations are indicated by curves and the experimental data are indicated by solid circles. The pink curves in (b) and (d) represent the added intensities of the lowest (red) and the second-lowest (blue) modes for the data of which the energies are close to each other. Similarly, the black curves in (b) and (d) are the results after adding all contributions from the four high-energy modes around 4 meV. (e) Schematics of spin fluctuation for each mode at 0 Oe. Transverse fluctuation in the $a$-$b$ plane is called the $T_1$ mode, those along the $c$ direction the $T_2$ mode, and longitudinal fluctuation the $L$ mode.

multiferroic device that switches the direction of the spin moment by a small electric field.

Professor A. Zheludev and Dr. S. Gvasaliya are greatly appreciated for facilitating the neutron scattering experiment and for fruitful discussion. This work was supported by KAKENHI (24340077, 20740171, 24740224, and 23540390).

*masuda@issp.u-tokyo.ac.jp

[1] G. A. Smolenskii and I. E. Chupis, Sov. Phys. Usp. **25**, 475 (1982).
[2] M. Fiebig, J. Phys. D **38**, R123 (2005).
[3] W. Eerenstein, N. D. Mathur, and J. F. Scott, Nature (London) **442**, 759 (2006).
[4] T. Kimura, T. Goto, H. Shintani, K. Ishizaka, T. Arima, and Y. Tokura, Nature (London) **426**, 55 (2003).
[5] H. Katsura, N. Nagaosa, and A. V. Balatsky, Phys. Rev. Lett. **95**, 057205 (2005).
[6] M. Mostovoy, Phys. Rev. Lett. **96**, 067601 (2006).
[7] I. A. Sergienko and E. Dagotto, Phys. Rev. B **73**, 094434 (2006).
[8] C. Jia, S. Onoda, N. Nagaosa, and J. H. Han, Phys. Rev. B **76**, 144424 (2007).
[9] T. Arima, J. Phys. Soc. Jpn. **76**, 073702 (2007).
[10] T. Sato, T. Masuda, and K. Uchinokura, Physica (Amsterdam) **329B–333B**, 880 (2003).
[11] A. Zheludev, T. Sato, T. Masuda, K. Uchinokura, G. Shirane, and B. Roessli, Phys. Rev. B **68**, 024428 (2003).
[12] H. Murakawa, Y. Onose, S. Miyahara, N. Furukawa, and Y. Tokura, Phys. Rev. Lett. **105**, 137202 (2010).
[13] H. Murakawa, Y. Onose, S. Miyahara, N. Furukawa, and Y. Tokura, Phys. Rev. B **85**, 174106 (2012).
[14] H. T. Yi, Y. J. Choi, and S. W. Cheong, Appl. Phys. Lett. **92**, 212904 (2008).
[15] J. M. Perez-Mato and J. L. Ribeiro, Acta Crystallogr. Sect. A **67**, 264 (2011).
[16] S. Bordács *et al.*, Nat. Phys. **8**, 734 (2012).
[17] J. Romhányi, M. Lajkó, and K. Penc, Phys. Rev. B **84**, 224419 (2011).
[18] K. Penc *et al.*, Phys. Rev. Lett. **108**, 257203 (2012).
[19] These representations can be also obtained by using the relation between the polarization **P**, spin moment **S**, and the position vector of ligands $\mathbf{e}_i$, $\mathbf{P} \propto \Sigma_i (\mathbf{S} \cdot \mathbf{e}_i)^2 \mathbf{e}_i$.
[20] S. Miyahara and N. Furukawa, J. Phys. Soc. Jpn. **80**, 073708 (2011).
[21] I. Kezsmárki, N. Kida, H. Murakawa, S. Bordacs, Y. Onose, and Y. Tokura, Phys. Rev. Lett. **106**, 057403 (2011).
[22] R. Shiina, H. Shiba, P. Thalmeier, A. Takahashi, and O. Sakai, J. Phys. Soc. Jpn. **72**, 1216 (2003).
[23] S. Sachdev and R. N. Bhatt, Phys. Rev. B **41**, 9323 (1990).
[24] J. Romhányi and K. Penc, Phys. Rev. B **86**, 174428 (2012).